Inorganic Chemistry
Cite This: Inorg. Chem. 2019, 58, 5886−5899
Article
pubs.acs.org/IC

Unraveling the Hidden Martensitic Phase Transition in BaClF and PbClF under High Pressure Using an Ab Initio Evolutionary Approach

N. Yedukondalu*[,†,‡] and M. Mahdi Davari Esfahani[†]

[†]Department of Geosciences, Center for Materials by Design, and Institute for Advanced Computational Science, State University of New York, Stony Brook, New York 11794-2100, United States

[‡]Rajiv Gandhi University of Knowledge Technologies, Basar, Telangana-504107, India

Supporting Information

ABSTRACT: We predict crystal structures of MClF (M = Ba and Pb) compounds by performing an ab initio evolutionary simulation at ambient as well as high pressure. We propose a structural transition sequence in MClF compounds as follows: $P4/nmm \rightarrow Pmcn \rightarrow P6_3/mmc$ below 100 GPa. The predicted ambient and intermediate phases are consistent with X-ray and Raman spectroscopic measurements, while the newly proposed high pressure $P6_3/mmc$ phase is thermodynamically more favorable than the previously proposed monoclinic ($P2_1/m$) phase. It is found that the $P4/nmm \rightarrow Pmcn$ transition is first order in nature, while the $Pmcn \rightarrow P6_3/mmc$ transition is a martensitic phase transition, which is accompanied by a slight volume change and is of a displacive nature. The austenite and martensite phases coexist in a wide pressure range, especially for PbClF. The martensite phase transition is mainly driven by (1) tilting and transformation of distorted heptahedron to pentahedron environment of MCl_6, which leads to negative area compressibility, and (2) cooperative displacive movement of F^- ions to form a trigonal bypyramidal (MF_5) structure around a metal cation. Overall, the metal cation coordination increases from 9 (MF_4Cl_5−$P4/nmm$) to 10 (MF_4Cl_6−$Pmcn$) and, further, to 11 (MF_5Cl_6−$P6_3/mmc$) under high pressure. The predicted ambient and high pressure phases are mechanically and dynamically stable under the studied pressure range. Electronic structure, bonding, and optical properties are calculated and discussed using new parametrization of Tran Blaha modified Becke Johnson potential. We find nearly isotropic optical properties (except for the ambient phase of PbClF), even though all the predicted ambient and high pressure phases are structurally anisotropic.

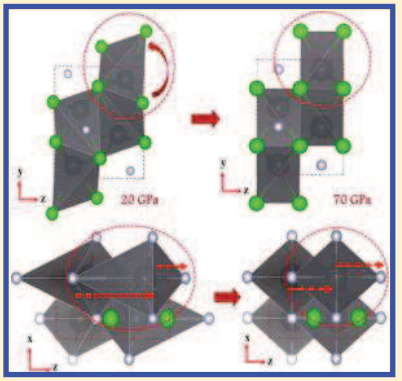

INTRODUCTION

MXY-type compounds (where M is a metal and X and Y are nonmetals) belong to a class of layered materials that crystallize in the primitive tetragonal ($P4/nmm$) symmetry at ambient conditions.[1] The MXY-type materials are classified into PbClF-type ($\frac{c}{a} < 2$ and $v(M) < 0.23$) and anti-Fe_2As[1] or ZrSiS-type[2,3] ($\frac{c}{a} > 2$ and $v(M) > 0.25$) based on $\frac{c}{a}$ and $v(M)$ (where $v(M)$ is a fractional coordinate of the metal atom). The PbClF-type compounds are wide band gap insulators/semicondutors with significant technological applications such as X-ray image storage phosphors[4,5] and pressure calibrants[6,7] in diamond anvil cells (DAC) upon doping with rare-earth ions and they also play an important role in spectroscopic and nuclear detectors. In contrast, ZrSiS-type compounds achieved tremendous interest recently due to their nodal-line semimetallic (NLSM) behavior at ambient conditions.[8] It is commonly expected that MXY-type materials exhibit anisotropic properties under high pressure due to their layered structure, which has been intriguing many researchers toward high pressure behavior of this class of materials. Therefore, extensive studies have been devoted to understand the high pressure behavior of PbClF-type materials. High pressure X-ray diffraction measurements on BaClF single crystals reveal that BaClF is stable up to 6.5 GPa, it has isotropic compressibility at 2 GPa, and later it becomes anisotropic.[9] Subramanian et al.[10] determined the structural stability of BaClF up to 35 GPa, and they observed a monoclinic ($P2_1/m$) phase at around 22 GPa. Later, high pressure X-ray diffraction measurements[11,12] on MClF (M = Ca, Sr, Ba) and BaBrF compounds reveal that BaClF and BaBrF undergo structural phase transitions at 21 and 27 GPa, respectively. Decremps et al.[13] also reported the high pressure behavior of BaIF and proposed that BaIF undergoes a structural phase transition at around 55 GPa. The pressure derivative of second order elastic constants of BaClF have been measured under hydrostatic pressure using ultrasonic pulse echo and Brillouin scattering techniques.[14] Anisotropic compressibilities of matlockite-type compounds (SrClF, SrBrF and PbBrF) are predicted at high pressure and no structural phase transitions were proposed up to 30 GPa for three compounds.[15] Liu et al.[16] predicted a structural phase

Received: January 24, 2019
Published: April 18, 2019

DOI: 10.1021/acs.inorgchem.9b00243
Inorg. Chem. 2019, 58, 5886−5899

transition from $P4/nmm$ to $P2_1/m$ in BaClF at 28.92 GPa based on molecular dynamics simulations.

Interestingly, a high pressure Raman spectroscopic study[17] on BaClF showed an intermediate orthorhombic ($Pnma$) phase at around 10.8 GPa which coexists with the ambient $P4/nmm$ phase and above 21.1 GPa these two phases coexist with the previously observed $P2_1/m$[10] phase up to the maximum studied pressure of 25.6 GPa. Subramanian et al.[18] also determined the high pressure behavior of BaBrF and BaIF compounds and confirmed the existence of an intermediate $Pnma$ phase for the iso-structural PbClF-type compounds. High pressure X-ray and Raman spectroscopic measurements on PbClF and PbBrF compounds[19,20] have shown similar structural transition trends, as observed in the case of BaXF (X = Cl, Br and I) compounds.[18] Hence, the observed structural transition sequence in these PbClF-type compounds is as follows: $P4/nmm \rightarrow Pnma \rightarrow P2_1/m$ under high pressure.[17−20] However, the crystal structure of an intermediate orthorhombic ($Pnma$) high pressure phase is unknown until date. Recently a high pressure structural phase transition sequence in ZrSiS (which is a prototype for anti-Fe_2As type materials) has been proposed based on the sequence observed in PbClF-type compounds using high pressure X-ray synchrotron and Raman spectroscopic measurements.[21] Determining crystal structures of coexisting phases at high pressure is always a challenging task for experimentalists.[22] This motivated us to predict the crystal structures of high pressure phases and structural transition sequence in PbClF-type compounds by taking the advantage of powerful and diversified evolutionary algorithm, which is implemented in Universal Structure Predictor: Evolutionary Xtallography (USPEX) package.[23−25]

In the present work, we resolved crystal structures of high pressure phases of PbClF and BaClF compounds that remained as an unsolved problem for the past two decades. We also predict the $Pnma \rightarrow P6_3/mmc$ transition to be martensitic and that the transition is associated with a slight volume change at the transition pressure going along with a displacive movement of ions to high symmetry Wyckoff positions to form a hexagonal-close-packed (hcp) structure. In addition, we have also calculated thermophysical properties of the predicted phases of MClF compounds under high pressure and discussed them in a detailed manner in the Results and Discussion section.

COMPUTATIONAL DETAILS AND METHODOLOGY

Our crystal structure prediction of MClF (M = Ba and Pb) matlockite-type compounds under high pressure has been carried out using the evolutionary algorithm USPEX.[23−25] We have done an extensive crystal structure search at ∼0, 10, 30, 60, and 100 GPa with 2, 4, and 8 formula units per primitive cell for both of the stduied compounds. The initial 100 structures are randomly generated and the succeeding 44 generations with a population size of 50 were obtained by applying heredity (50%), random (20%), soft mutation (20%), and lattice mutation (10%) operators until the best structure remains invariant up to 20 generations. The Vienna Ab Initio Simulation Package (VASP)[26] has been used as an external density functional theory (DFT) package to perform structural relaxations to explore the global minimum energy structure of the investigated compound at a given pressure. Geometry optimization and lattice dynamical properties were calculated with projector-augmented plane-wave (PAW) potentials[27] with $5s^25p^66s^2$, $5d^{10}6s^26p^2$, $2s^22p^5$, and $3s^23p^5$ electrons treated as valence states for Ba, Pb, F, and Cl, respectively. Electron−electron interactions were treated within the generalized gradient approximation of the Perdew−Burke−Ernzerhof (PBE) parametrization.[28] A kinetic energy cutoff of 560 eV was used for the plane wave basis set expansion and also $2\pi \times 0.2$ Å^{-1} k-spacing has been chosen to sample the Brillouin zone after performing careful convergence tests w.r.t. total energy. In order to perform lattice dynamical and elastic constants calculations, the total energy and forces are converged to smaller than 10^{-8} eV and 10^{-4} eV/Å, respectively, during the structural relaxation. The lattice dynamical calculations were carried out using the supercell approach as implemented in VASP[26] and postprocessing using the PHONOPY.[29] To ensure sufficient atomic interactions, we have chosen the lattice constants of supercell between 12 and 15 Å along each crystallographic direction to obtain real phonon frequencies for each phase of the investigated compounds with Monkhorst−Pack[30] k-mesh sampling of $2 \times 2 \times 2$.

The pressure dependent elastic constants of MClF compounds are calculated using a recently developed in house Finite Pressure Temperature Elasticity (FPTE) package,[31] which applies strain deformations based on crystal symmetry, and the corresponding stress tensor is calculated by interfacing with VASP. The FPTE package includes pressure correction to the computed elastic constants at finite pressure (the methodology will be published elsewhere).

Electronic structure and optical properties of BaClF and PbClF were calculated using the new parametrization of Tran Blaha-modified Beche Johnson (TB-mBJ)[32] potential, which is implemented in the WIEN2k package[33] (for more details, see section I of the Supporting Information). The new parametrization of TB-mBJ potential is obtained by optimizing the parameter "c" (see Table 2 of ref 34 for different set of α and β values to obtain "c" value for various new parametrizations of the TB-mBJ potential), namely, original TB-mBJ,[32] p-present (TB-mBJ:1), and p-semiconductor (TB-mBJ:2), and among them, TB-mBJ:2 parametrization works better for semiconductors up to 7 eV.[34]

RESULTS AND DISCUSSION

Crystal Structure Prediction under High Pressure. Determining the crystal structure of high pressure phases for PbClF-type compounds is a challenging problem for researchers from the last two decades. Furthermore, they are substantial in understanding the structural phase transformations in ZrSiS-type[21] materials under high pressure. The ZrSiS-type materials are NLSMs at ambient pressure, which makes them stars of this particular research field due to linear band inversion along high symmetry directions of the Brillouin zone to form nodal loops.[8,21] The knowledge on crystal structures of PbClF-type compounds at high pressure not only provides an insight on their phase diagrams, but also, they are crucial in understanding the high temperature superconductivity of ZrSiS-type materials.[21] In order to address this problem, we made an extensive crystal structure search at different pressures for BaClF and PbClF compounds. The predicted ambient tetragonal ($P4/nmm$) and intermediate ($Pmcn$) phases are in excellent agreement with the experiments.[17−20] Based on the enthalpy calculations, we also propose a new transition from $Pmcn$ ($Pnma$) $\rightarrow P6_3/mmc$, in contrast to the transition from $Pnma \rightarrow P2_1/m$, as observed in the experiments at high pressure for BaClF and PbClF. In order to confirm the proposed new transition sequence, we performed a fixed cell prediction with the determined monoclinic ($P2_1/m$, with $Z = 2$ f.u./cell) lattices M1 and M2 for BaClF[10] and PbClF[20] from powder X-ray diffraction measurements. The predicted fractional coordinates

DOI: 10.1021/acs.inorgchem.9b00243
Inorg. Chem. 2019, 58, 5886−5899

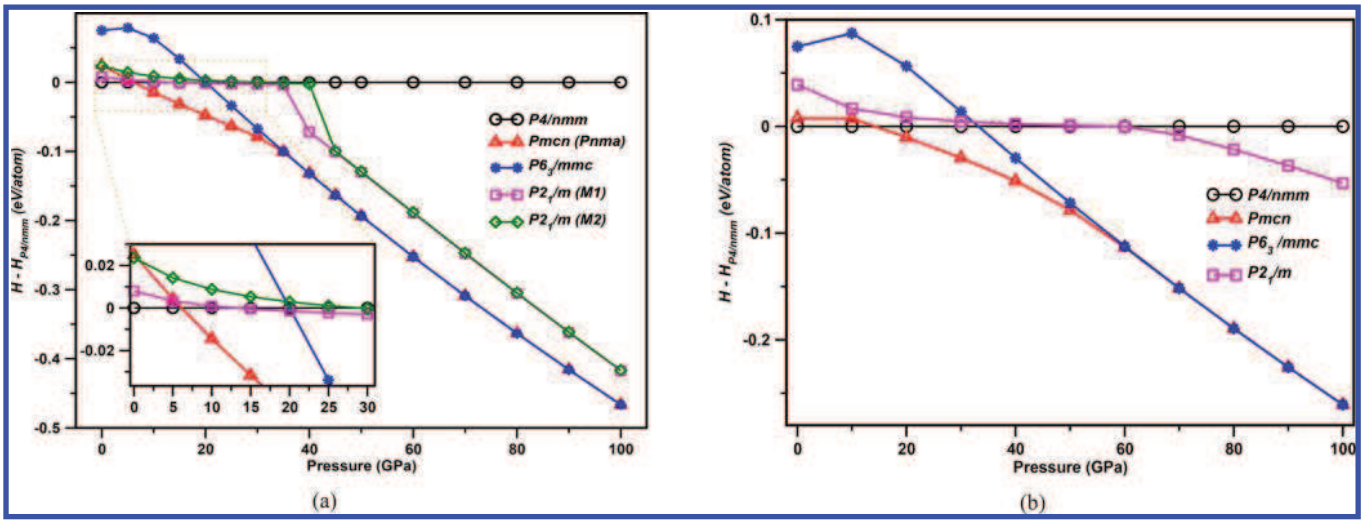

Figure 1. Calculated relative enthalpy difference of high pressure phases of (a) BaClF and (b) PbClF compounds as a function of pressure w.r.t. *P4/nmm* (ambient) phase. Predicted structural transition sequence under high pressure is $P4/nmm \rightarrow Pmcn \rightarrow P6_3/mmc$ in both of these compounds. The $P6_3/mmc$ phase is found to be energetically favorable compared to the experimentally claimed monoclinic ($P2_1/m$) phase. $Pmcn \rightarrow P6_3/mmc$ phase transition is a martensitic phase transition that is a weak first order transition with displacive nature. The austenite and martensite phases coexist in a wide pressure range.

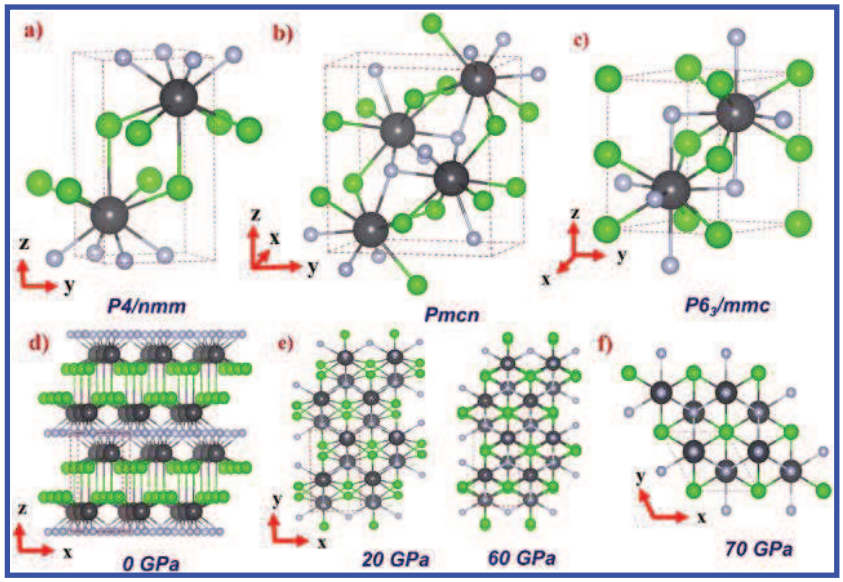

Figure 2. Crystal structures of ambient and high pressure phases of PbClF. The black, green, and ash color balls represent Pb, Cl, and F atoms, respectively. (a, d) Layered crystal structure of the ambient ($P4/nmm$) phase and the layers Cl^--Pb^{2+}-F^--F^--Pb^{2+}-Cl^- are stacked along the *c*-axis. (b, e) Crystal structure of an intermediate ($Pmcn$) phase with distorted hexagon in the *ab*-plane at 20 and 60 GPa. (c, f) Hexagonal close packed crystal structure of high pressure ($P6_3/mmc$) phase with an ideal hexagon in the *ab*-plane.

of monoclinic phases of BaClF and PbClF, along with the determined lattice constants, are summarized in Table S1. As illustrated in Figure 1, the relative enthalpy difference of ambient and high pressure phases, including M1 and M2 lattices, clearly demonstrates that the $P4/nmm \rightarrow Pmcn$ phase transition is first order in nature, which is in good agreement with the experimentally proposed intermediate orthorhombic *Pnma* phase for MXF (M = Ba, Pb; X = Cl, Br)[17−20] and BaIF[18] compounds. The calculated transition pressures 6.1 and 14.2 GPa for the $P4/nmm \rightarrow Pmcn$ transition are slightly underestimated when compared to the experimental transition pressures at ∼10.8[17] and ∼18 GPa[19] for BaClF and PbClF, respectively. The second phase transition is from $Pmcn \rightarrow P6_3/mmc$, rather than from *Pnma* ($Pmcn$) → $P2_1/m$, since the $P6_3/mmc$ phase has a lower enthalpy (∼60 meV/atom over $P2_1/m$ phase at 40 GPa), which implies that the predicted $P6_3/mmc$ phase is energetically more favorable than the experimentally determined $P2_1/m$ phase at high pressure for BaClF[10] and PbClF.[20] In addition, by comparing the measured Raman spectra at two distinct pressures, 33 and 41 GPa, it is clearly observed that the intermediate (*Pnma*) phase favors to develop a high symmetry structure rather than a low symmetry monoclinic ($P2_1/m$) structure under high pressure (see Figure 2 of ref 19). Moreover, the $Pmcn \rightarrow P6_3/mmc$ transition shows a very weak volume collapse at the transition pressure, which is accompanied by cooperative displacive movements of (Ba/Pb, F, and Cl) atoms to highly symmetric Wykcoff positions (mainly Cl: 0.68 → 0.75; F: 0.35 → 0.25 for BaClF and Cl: 0.82 → 0.75; F: 0.20 → 0.25 for PbClF) to form an ideal hexagon ($P6_3/mmc$) instead of distorted ones ($Pmcn$), as illustrated in Figure 2e,f. This type

DOI: 10.1021/acs.inorgchem.9b00243
Inorg. Chem. 2019, 58, 5886−5899

of transition is called martensitic phase transformation, as observed in the case of steel (irreversible)[35] and shape memory alloys (reversible).[36] Bhattacharya et al.[37] proposed a criteria for reversibility of martensitic phase transitions based on crystal symmetry of austenite and martensite phases, if energy barrier to lattice invariant shear is higher than barrier to the phase change with no plasticity then it is reversible martensitic phase transition. Austenite and martensite phases should have a group−subgroup relationship, which is a necessary condition for reversibility, as seen in shape memory alloys.[36] The predicted intermediate *Pmcn* and high pressure $P6_3/mmc$ phases are sub- and supergroups of the *Cmcm* space group, respectively. According to the Hermann theorem, there exists a group−subgroup relationship between *Pmcn* and $P6_3/mmc$ phases through an intermediate *Cmcm* space group in two steps: (1) *Pmcn* is the klassengleiche subgroup of *Cmcm* space group, since the two space groups have same point groups, and (2) *Cmcm* is the translationengleich subgroup of $P6_3/mmc$ space group, since they have the same group of translations. In the first step, the centering is achieved as a function of pressure in *Pmcn* symmetry, that is, a C-centered orthorhombic (*Cmcm*) lattice that raises the translations, but the point groups remain the same, that is, the klassengleiche subgroup. In the second step, the hexagonal symmetry is achieved by removing the distortion in the C-centered lattice to form a hexagonal symmetry without changing the group of translations, that is, the translationengleich subgroup. Therefore, there exists a maximal group−subgroup relationship between *Pmcn* and $P6_3/mmc$ space groups. This clearly indicates that the *Pmcn* → $P6_3/mmc$ transition is a reversible martensite phase transition through the group−subgroup relationship criteria proposed by Bhattacharya et al.[37] Although the experimentally proposed high pressure ($P2_1/m$) phase is unlike that in the present study, a reversible structural transition is observed in the high pressure X-ray powder diffraction measurements for MClF (M = Ca, Sr, and Ba and Cl, Br, and I) compounds.[10,17−20] It is very interesting to disclose pressure-induced martensitic phase transition in this PbClF-type class of materials. Moreover, the *Pmcn* → $P6_3/mmc$ transition is previously reported for perovskite $NaMgF_3$, and this was predicted by compressing the postperovsikte (*Cmcm*) structure to ultrahigh high pressure.[38−40]

In addition, we could see subtle differences between the obtained and experimental transition pressures (although the observed high pressure monoclinic ($P2_1/m$) phase differs from the predicted hcp $P6_3/mmc$ phase in this work) for both of these compounds. This may be due to austenite (*Pmcn*) and martensite ($P6_3/mmc$) phases coexisting in a wide pressure range, ∼28−40 GPa for BaClF and ∼45−70 GPa for PbClF, which is an inherent characteristic of martensitic phase transition.[37] Therefore, it becomes a tedious task for experimentalists to determine the correct crystal symmetry of mixed phases in general and PbClF-type compounds in particular under high pressure. The *Pmcn* phase completely transforms to the $P6_3/mmc$ phase above ∼35 GPa for BaClF and ∼70 GPa for PbClF, as depicted in Figure 1.

The analysis of the crystal structure and the bond parameters (bond lengths and/or angles) provide good insight on coordination numbers for ambient and high pressure phases. As discussed in section I, the PbClF-type compounds crystallize in the primitive tetragonal ($P4/nmm$) symmetry with two formula units per unit cell at ambient conditions. The metal (Pb/Ba), chlorine, and fluorine atoms are located at 2*c* and 2*a* wykcoff positions, respectively. The Pb^{2+} cation is coordinated by 4-fold F^- and 5-fold Cl^- ions, resulting in a PbF_4Cl_5 structural motif that has a C_{4v} site symmetry with 9-fold coordination in PbClF-type compounds at ambient pressure.[41] The 4-fold coordination of F^- and Cl^- ions form a square planar structure on above and below the Pb^{2+} (metal) cation, respectively, and vice versa to form a layered structure in the unit cell with $Z = 2$ f.u., and the Cl^--Pb^{2+}-F^--F^--Pb^{2+}-Cl^- layers in the unit cell are stacked along the *c*-axis, as shown in Figure 2d. Therefore, PbClF-type compounds are layered materials with a quasi-2D character at ambient conditions.[42,43] In addition, the *c*-axis is found to have larger compressibility when compared to the *a*-axis for the ambient phase due to weakly stacked layers along the *c*-direction, which clearly shows the weaker interlayer bonding over intralayer bonding in the MClF compounds in $P4/nmm$ symmetry. Application of hydrostatic pressure on PbClF-type compounds slightly distorts the square planar nature of both F^- and Cl^- ions (which are perpendicular to the *c*-axis for the ambient phase) around the Pb^{2+} cation, which eventually effects the layered nature of this class of materials under high pressure. For the intermediate (*Pmcn*) and high pressure ($P6_3/mmc$) phases, the Pb^{2+} cation is coordinated by a 4-fold and 5-fold trigonal bipyramidal structure of F^- ions along with 6-fold Cl^- ions environment to form PbF_4Cl_6 and PbF_5Cl_6 structural motifs, resulting in coordination numbers (CNs) 10 and 11, respectively. Overall, the CN increases from 9 to 10 and further to 11 for $P4/nmm$, *Pmcn*, and $P6_3/mmc$ phases under high pressure, respectively (see Figure 3). The increase in CN

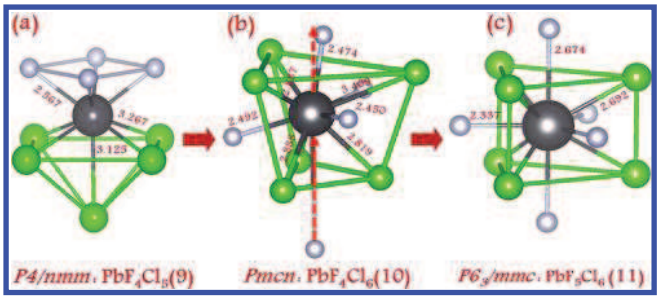

Figure 3. Coordination number (CN) of Pb^{2+} cation in the predicted (a) ambient ($P4/nmm$) phase with 4-fold F^- and 5-fold Cl^- ions in a square planar around a Pb^{2+} cation, which forms a perfect layered structure with a structural motif PbF_4Cl_5. (b) An intermediate (*Pmcn*) phase with 4-fold F^- and 6-fold Cl^- around a Pb^{2+} cation with a structural motif PbF_4Cl_6. (c) High pressure ($P6_3/mmc$) phase with 5-fold F^- and 6-fold Cl^- around a Pb^{2+} cation with a structural motif PbF_5Cl_6. The same color convention is followed, as given in Figure 2, for representation of atoms.

resulting from the coordination environment of Cl (PbF_4Cl_5 → PbF_4Cl_6) and F (PbF_4Cl_6 → PbF_5Cl_6) ions around the metal cation during the $P4/nmm$ → *Pmcn* and *Pmcn* → $P6_3/mmc$ phase transitions, respectively. In addition, the *Pmcn* phase of the MClF compounds has a slightly less distorted hexagon-like arrangement, as depicted in Figure 2d. Upon further compression of the *Pmcn* phase, the M (Ba or Pb), F, and Cl atoms are displaced to a highly symmetric position (see Figure 4) that mostly drives the transition from the *Pmcn* to a $P6_3/mmc$ (hcp) structure under high pressure, which forms an ideal hexagon.

The predicted structural properties for three phases at different pressures are presented in Table 1 and are in good agreement with the available experimental[12,44−46] data as well as with previous theoretical calculations at ambient pressure.[41,47,48]

DOI: 10.1021/acs.inorgchem.9b00243
Inorg. Chem. 2019, 58, 5886−5899

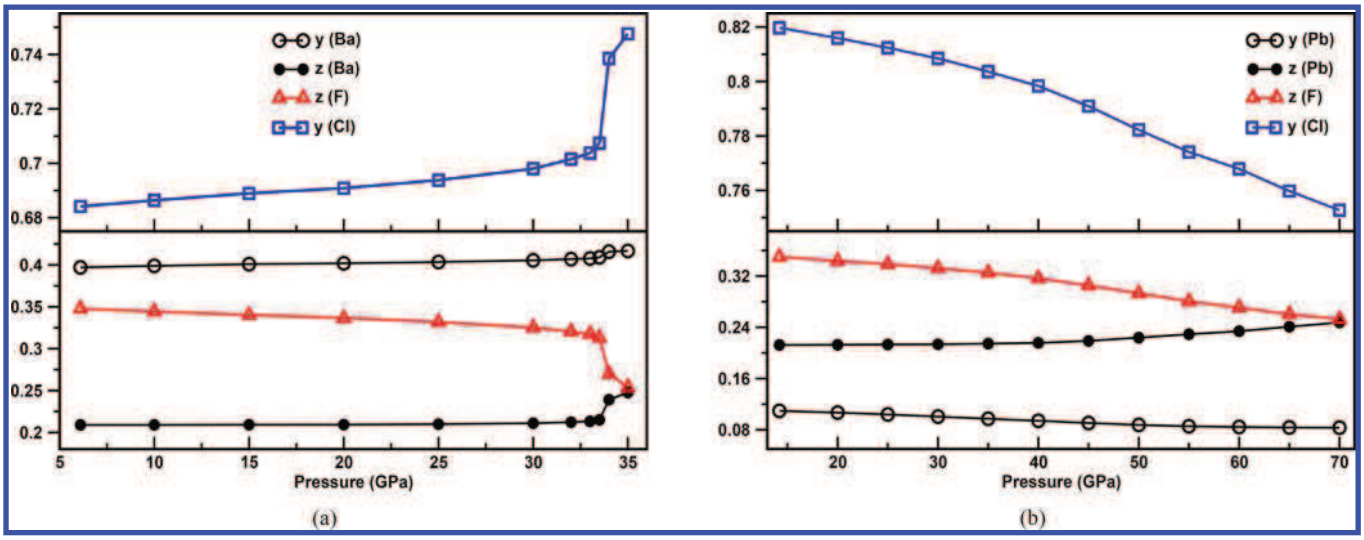

Figure 4. Variation of fractional coordinates of intermediate (*Pmcn*) phase as a function of pressure for (a) BaClF and (b) PbClF compounds. The (Ba/Pb, Cl, and F) atoms show a displacive nature to high symmetry wykcoff positions (Ba: 0.213 → 0.25; Cl: 0.68 → 0.75; F: 0.35 → 0.25 for BaClF and Pb: 0.21 → 0.25; Cl: 0.82 → 0.75; F: 0.20 → 0.25 for PbClF).

Table 1. Predicted Lattice Constants and Fractional Coordinates of Ambient and High Pressure Phases of BaClF and PbClF and Compared with the Experimental Data for Ambient Phases of the Both Investigated Compounds

method	phase	BaClF	PbClF
this work	*P*4/*nmm* (0 GPa)	a = 4.454, c = 7.357	a = 4.167, c = 7.376
		Ba: 2*c* (0.25, 0.25, 0.2051)	Pb: 2*c* (0.25, 0.25, 0.2053)
		Cl: 2*c* (0.25, 0.25, 0.6469)	Cl: 2*c* (0.25, 0.25, 0.6482)
		F: 2*a* (0.75, 0.25, 0.0000)	F: 2*a* (0.75, 0.75, 0.0000)
expt		a = 4.394[a]/4.3964[b], c = 7.225[a]/7.2315[b]	a = 4.110[c], 7.246[c]
		Ba: 2*c* (0.25, 0.25, 0.2049[a] /0.2063[b])	Pb: 2*c* (0.25, 0.25, 0.2058)[c]
		Cl: 2*c* (0.25, 0.25, 0.6472[a] /0.6466[b])	Cl: 2*c* (0.25, 0.25, 0.6497)[c]
		F: 2*a* (0.75, 0.25, 0.0000)[a,b]	F: 2*a* (0.75, 0.75, 0.0000)[c]
this work	*Pmcn*	a = 4.336, b = 7.309, c = 6.907	a = 4.075, b = 7.279, c = 6.668
	(20 GPa)	Ba: 4*c* (0.25, 0.4019, 0.2093)	Pb: 4*c* (0.25, 0.1068, 0.2127)
		Cl: 4*c* (0.25, 0.6908, 0.5032)	Cl: 4*c* (0.25, 0.8159, 0.4920)
		F: 4*c* (0.25, 0.0778, 0.3366)	F: 4*c* (0.25, 0.4273, 0.3437)
	$P6_3/mmc$	a = 4.235, c = 5.312	a = 4.047, c = 5.349
	(70 GPa)	Ba: 2*c* (0.3333, 0.6667, 0.25)	Pb: 2*c* (0.3333, 0.6667, 0.25)
		Cl: 2*a* (0.0000, 0.0000, 0.00)	Cl: 2*a* (0.0000, 0.0000, 0.00)
		F: 2*d* (0.6667, 0.3333, 0.25)	F: 2*d* (0.6667, 0.3333, 0.25)

[a]Ref 12. [b]Ref 45. [c]Ref 46.

The predicted lattice constants and fractional coordinates of the intermediate phase are given in the more generalized space group *Pnma* in Table S2 which might serve as reference for future high pressure X-ray diffraction measurements. We have calculated the pressure dependence of in-equivalent bond lengths of each phase to get more insight on structural phase transformations in these materials. As depicted in Figure 5 and Table 2, the calculated bond lengths are decreasing with pressure except for *Pmcn* which shows a sharp decrease/increase in the bond lengths, especially close to the transition pressure, which is reflected in the lattice constants, as shown in Figure 6, which is more predominant in BaClF over PbClF. Interestingly, (Pb/Ba)−F(2) and (Pb/Ba)−Cl(1) bond lengths of *Pmcn* phase are increasing with pressure. The increase in (Ba/Pb)−F(2) bond length and cooperative displacive movement of F^- ions (as shown in Figure 3b) leads to formation of trigonal bypyramidal structure (see Figure 3c) to form an ideal hexagons from the distorted ones. This might be an indirect indication for the intermediate (orthorhombic) phase to undergo a high symmetry (hexagonal) structure rather than a low symmetry monoclinic ($P2_1/m$) structure under high pressure. We have also studied the pressure dependence of lattice constants and they decrease monotonically with pressure for all three phases except for *Pmcn* phase in which lattice constants *a*, *b*, and *c* show abnormal behavior in the pressure range 30−35 GPa for BaClF and 40−70 GPa for PbClF (see Figure 6). The lattice constants *a*, *b*, and *c* increase and decrease in such a way that the orthorhombic (lattice with Z = 4 f.u.) lattice constants *a* and *b* become lattice constant *a* of the hexagonal lattice (with Z = 2 f.u.). Moreover, both of the lattice constants *a* and *b* of *Pmcn* phase shows negative linear compressibility (NLC) in the pressure range of 30−35 and 40−70 GPa for BaClF and PbClF, respectively, that is, expansion of the *Pmcn* lattice in the *ab*-plane, resulting in a negative area of compressibility (NAC), as illustrated in Figure 6. In order to get deeper insight on NAC, we have analyzed the variation of a coordination environment of the anions around the metal cation at different pressures, which clearly demonstrates that a distorted heptahedron coordination

DOI: 10.1021/acs.inorgchem.9b00243
Inorg. Chem. 2019, 58, 5886−5899

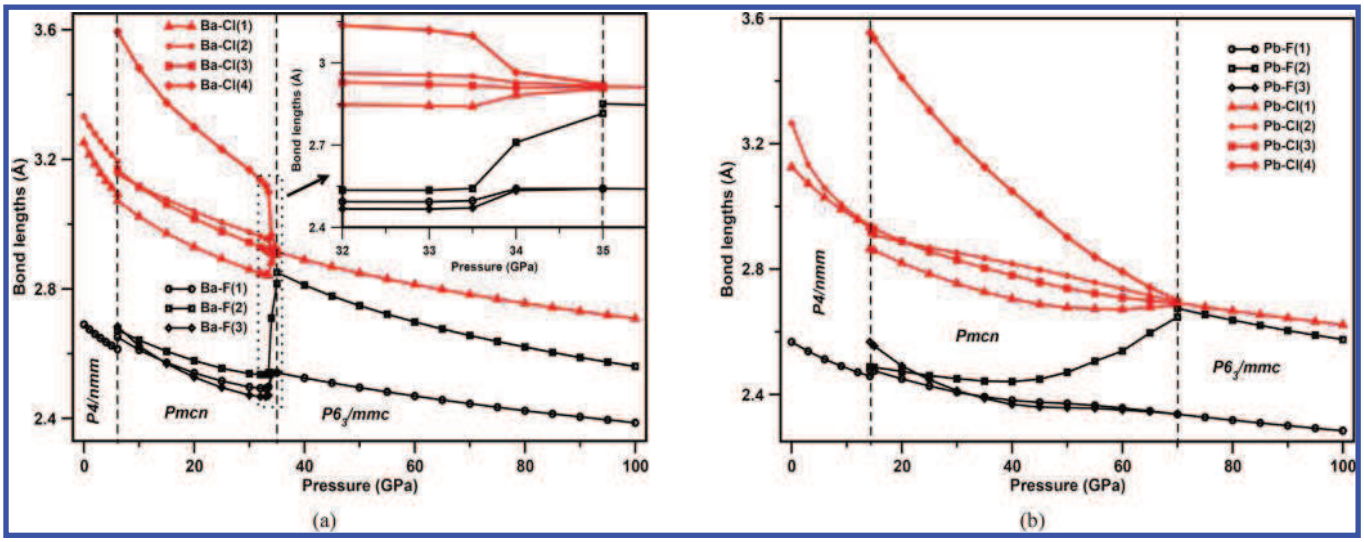

Figure 5. Calculated bond lengths for ambient and high pressure phases of (a) BaClF and (b) PbClF compounds. Merging of the lattice constants (see Figure 6) and bond parameters for BaClF and PbClF at around 35 and 70 GPa, respectively, clearly demonstrate that the *Pmcn* phase undergoes a high symmetry structure under high pressure.

Table 2. Calculated Inequivalent Bond Lengths of Ambient (*P4/nmm* at 0 GPa) and High Pressure (*Pmcn* at 20 GPa and $P6_3/mmc$ at 70 GPa) Phases of BaClF and PbClF Compounds

compound	bond length	*P4/nmm*	*Pmcn*	$P6_3/mmc$
BaClF	Ba−F(1)	2.690	2.540	2.445
	Ba−F(2)		2.578	2.656
	Ba−F(3)		2.527	
	Ba−Cl(1)	3.250	2.930	2.783
	Ba−Cl(2)	3.333	3.039	
	Ba−Cl(3)		3.017	
	Ba−Cl(4)		3.299	
PbClF	Pb−F(1)	2.567	2.450	2.337
	Pb−F(2)		2.474	2.674
	Pb−F(3)		2.492	
	Pb−Cl(1)	3.125	2.819	2.692
	Pb−Cl(2)	3.267	2.887	
	Pb−Cl(3)		2.888	
	Pb−Cl(3)		3.409	

environment formed by Cl^- ions around metal cation (see Figure 7) is tilting with increasing pressure to form a square planar structure perpendicular to the *y*-axis, which is responsible for NAC of the *Pmcn* lattice in MClF compounds under high pressure. Up on further compression, the distorted heptahedron transformed to a pentahedron environment of Cl^- ions in such way that they form an ideal hexagon with a M/F/Cl atom at the center. On the other hand, the *Pmcn* phase lattice constant *c* continues to be a hexagonal lattice constant *c* for the $P6_3/mmc$ phase. However, the lattice constant *c* exhibits large compressibility close to the transition (*Pmcn* → $P6_3/mmc$) pressures due to the cooperative displacive nature of F^- ions (see Figure 3b,c) to form a trigonal bypyramidal coordination environment around the metal cation, as illustrated in Figure 8. The primitive basis vectors of the $P6_3/mmc$ lattice in terms of the *Pmcn* lattice constants expressed as follows:

$$\begin{bmatrix} a_{P6_3/mmc} \\ b_{P6_3/mmc} \\ c_{P6_3/mmc} \end{bmatrix} = \begin{bmatrix} 1 & 0 & 0 \\ -\frac{1}{2} & \frac{1}{2} & 0 \\ 0 & 0 & 1 \end{bmatrix} \times \begin{bmatrix} a_{Pmcn} \\ b_{Pmcn} \\ c_{Pmcn} \end{bmatrix}$$

Furthermore, to explore the structural transition mechanism from *Pmcn* to $P6_3/mmc$, we have calculated the similarity parameters such as lattice distortion (S), maximum (d_{max}) and average (d_{avg}) atomic displacements and measure of similarity or structural descriptor (Δ) for *Pmcn* phase as a function of pressure, as illustrated in Figure 9. The similarity parameters are calculated by comparing structure at a given pressure with the reference structure at 35 GPa for BaClF and 70 GPa for PbClF using the *COMPSTRU* program.[49] The similarity between the lattice parameters of two structures (considered for comparison) is measured by "S", which is sum of the squared eigenvalues of the strain tensor divided by 3.[50] The atomic displacement field between the matched sites of the two structures can be measured by the d_{max} and d_{avg}. The (maximal) displacement between the atomic positions of the paired atoms is given by (d_{max}) *d* and the average atomic displacements summed over the primitive cell is given by d_{avg}.[49,51] The d_{max} is from the paired F atoms for both of BaClF and PbClF compounds, which is consistent with the cooperative displacive nature of F atoms (see Figures 8 and 3b). In addition, the atomic displacements of paired Cl atoms also closely comparable with the d_{max} of F atoms along with a small contribution from the metal (Ba/Pb) atoms. The Δ is a function of the differences in atomic positions (weighted by the multiplicities of the sites) and the ratios of the corresponding lattice parameters of the compared structures.[52] Therefore, the Δ is resulting from both lattice distortion and atomic displacements, which decreases with pressure, and it has a sharp decrease in the pressure range 33−34 GPa, especially for BaClF and 40−70 GPa for PbClF. This clearly indicates that the *Pmcn* → $P6_3/mmc$ transition is driven by the reduction of lattice distortion of *Pmcn* with atomic cooperative displacive movements, as demonstrated in Figures 7 and 8.

We have also calculated the volume of each predicted phase as a function of pressure which shows a monotonic decrease in the volume as a function of pressure, as presented in Figure 10. We could clearly see a volume collapse of ∼2.8% at 6.1 GPa for BaClF and ∼1.6% at 14.2 GPa for PbClF during the phase transition from *P4/nmm* → *Pmcn* phase while very weak volume collapse during *Pmcn* → $P6_3/mmc$ transition for both of the

DOI: 10.1021/acs.inorgchem.9b00243
Inorg. Chem. 2019, 58, 5886−5899

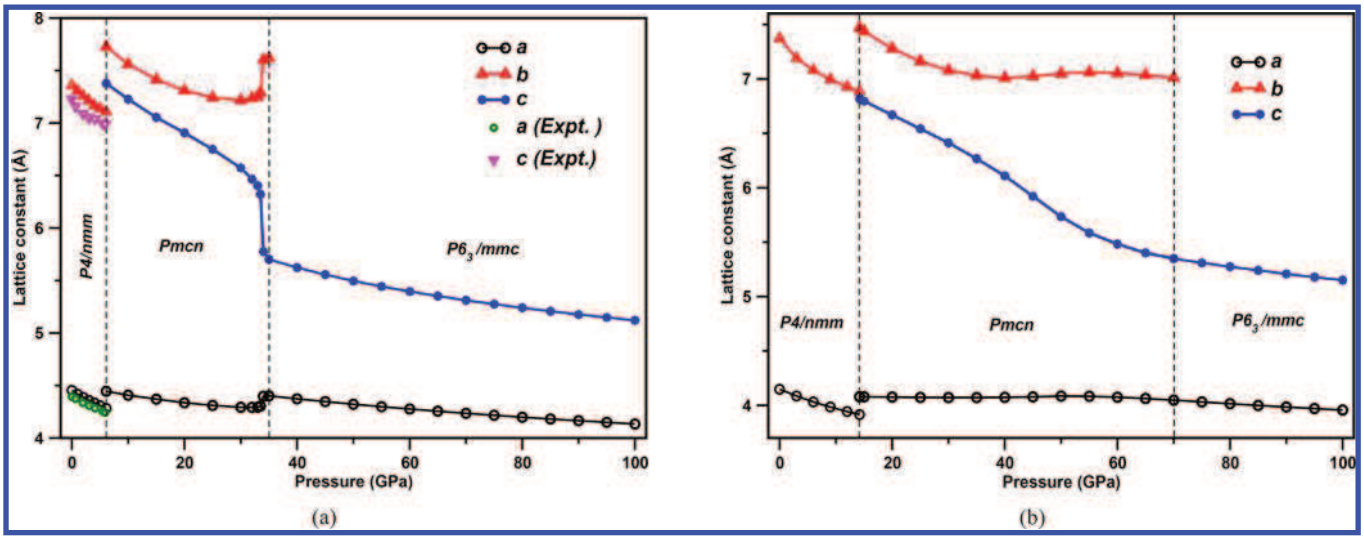

Figure 6. Calculated equilibrium lattice constants as a function of pressure for ambient and high pressure phases of (a) BaClF and (b) PbClF compounds. The lattice constants *a* and *b* of the *Pmcn* phase are merging into lattice constant *a* for the $P6_3/mmc$ phase, and the lattice constant *c* remains as *c* in both austenite and martensite phases for both of the studied compounds.

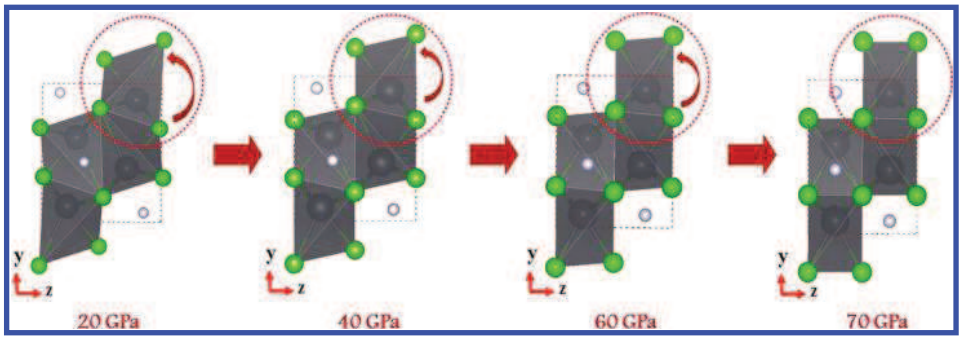

Figure 7. Tilting and transformation of the distorted heptahedron to pentahedron Cl^- ions environment around a Pb^{2+} cation as a function of pressure for *Pmcn* phase, which leads to negative area compressibility.

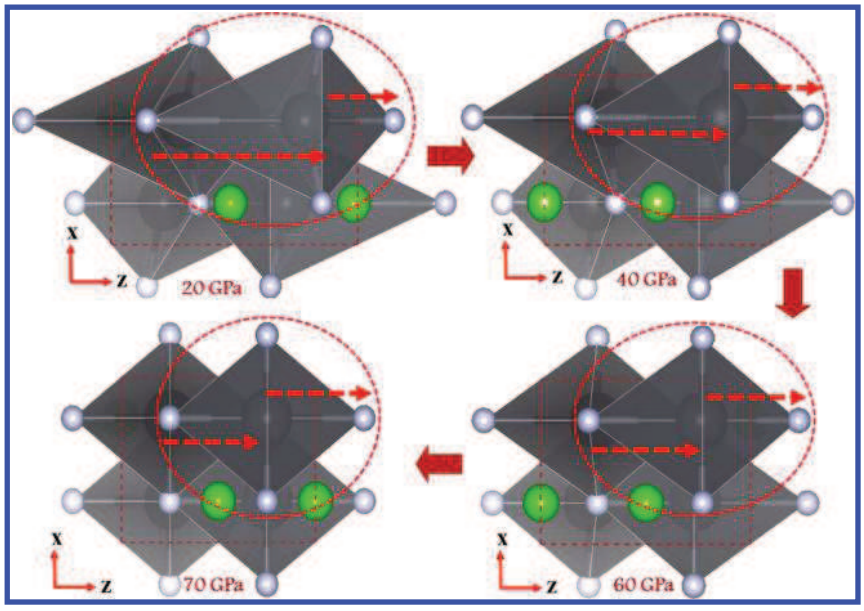

Figure 8. Cooperative displacive movement of F^- ions as a function of pressure for the *Pmcn* phase to form a trigonal bypyramidal structure environment around a Pb^{2+} cation leads to large compressibility of *c*-axis.

studied compounds. We have also obtained the equilibrium bulk modulus (B_0) and its pressure derivative (B_0') for each predicted phase by fitting total energy−volume (E−V) data to 3rd order Birch−Murnaghan equation of state. The obtained B_0 and B_0' for

DOI: 10.1021/acs.inorgchem.9b00243
Inorg. Chem. 2019, 58, 5886−5899

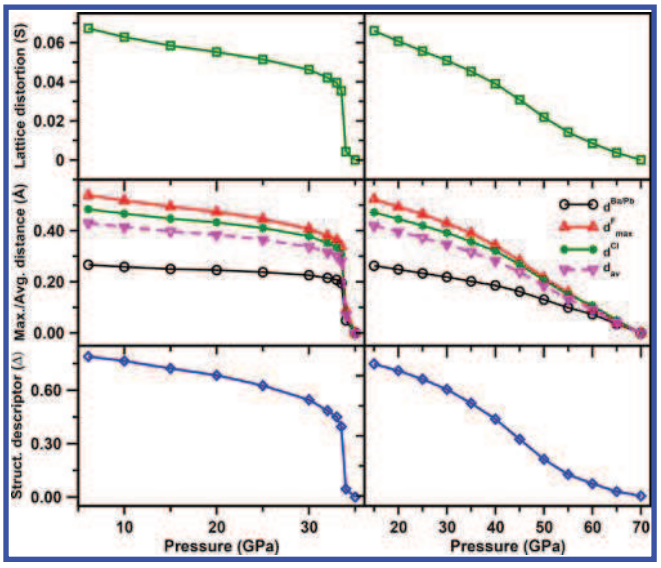

Figure 9. Calculated lattice distortion (S), maximum (d_{max}) and average (d_{avg}) distance and structural descriptor (Δ) of *Pmcn* phase as a function of pressure by taking reference structure at 35 GPa for BaClF and 70 GPa for PbClF.

ambient phase of both BaClF and PbClF compounds are consistent with experimental data and other theoretical calculations and all the results are summarized in Table 3 along with B_0 and B_0' values for the predicted high pressure phases. Moreover, the obtained B_0 and B_0' values for ambient and high pressure phases are compared with the polycrystalline aggregate bulk modulus (derived from single crystal elastic constants) using Voigt−Reuss−Hill approximation (see Table S3). Relatively low magnitude (~50 GPa) of B_0 values for both of the investigated compounds shows soft nature of these materials at ambient pressure.

Mechanical and Dynamical Stability under High Pressure. In order to get insight on strength of inter- and/or intramolecular interactions and mechanical stability of MClF compounds, we have computed the second order elastic constants at ambient as well as at high pressure using FPTE package. The predicted ambient and high pressure phases possess tetragonal, orthorhombic, and hexagonal crystal symmetries and correspondingly they have 6, 9, and 5 independent elastic constants, respectively. The calculated elastic constants for BaClF at ambient pressure are compared with the available elastic constants obtained from Ultrasonic and Brillouin zone pulse echo measurements,[53,54] and there is a good agreement between them (see Table S4), which shows the reliability of our FPTE package. The experimental trends are very well reproduced in this work with in the limitation of standard PBE-GGA functional when compared to the obtained elastic constants using local density approximation,[55] which implies that GGA functional outperforms LDA functional for BaClF.[41] The predicted phases are found to be mechanically stable at ambient as well as at high pressures. The pressure-dependent elastic constants increase with pressure for three predicted phases of BaClF and PbClF. As illustrated in Figure 11, merging of C_{11} and C_{22} axial, C_{44}, C_{55}, and C_{66} shear, and C_{13} and C_{23} dilation elastic constants of the *Pmcn* phase at the transition pressure for both of the studied compounds, resulting in five independent elastic constants for the hcp phase that is reflected from the pressure evolution of bond parameters and lattice constants, as illustrated in Figures 5 and 6, respectively.

To explore the dynamical stability of newly predicted high pressure phases of MClF compounds along with experimentally known ambient phase, we have computed the phonon dispersion curves along high symmetry directions of the

Table 3. Calculated Equilibrium Bulk Modulus of BaClF and PbClF Compounds are Compared with Available Experimental and Theoretical Calculations

compound	BaClF		PbClF	
phase	B_0	B_0'	B_0	B_0'
P4/nmm (this work)	39.7	5.8	44.6	7.1
expt	42,[a,b] 45,[b] 44,[c] 62[d]	4.5,[a] 6,[b] 5.8[c]	51[e]	5.6[e]
others	55.5,[f] 51.6[g]	4[f]		
Pmcn (*Pnma*)	38.9	7.0	29.4	9.4
$P6_3/mmc$	44.0	7.1	53.3	6.2

[a]Ref 9. [b]Ref 12. [c]Ref 14. [d]Ref 11. [e]Ref 20. [g]Ref 55. [f]Ref 56.

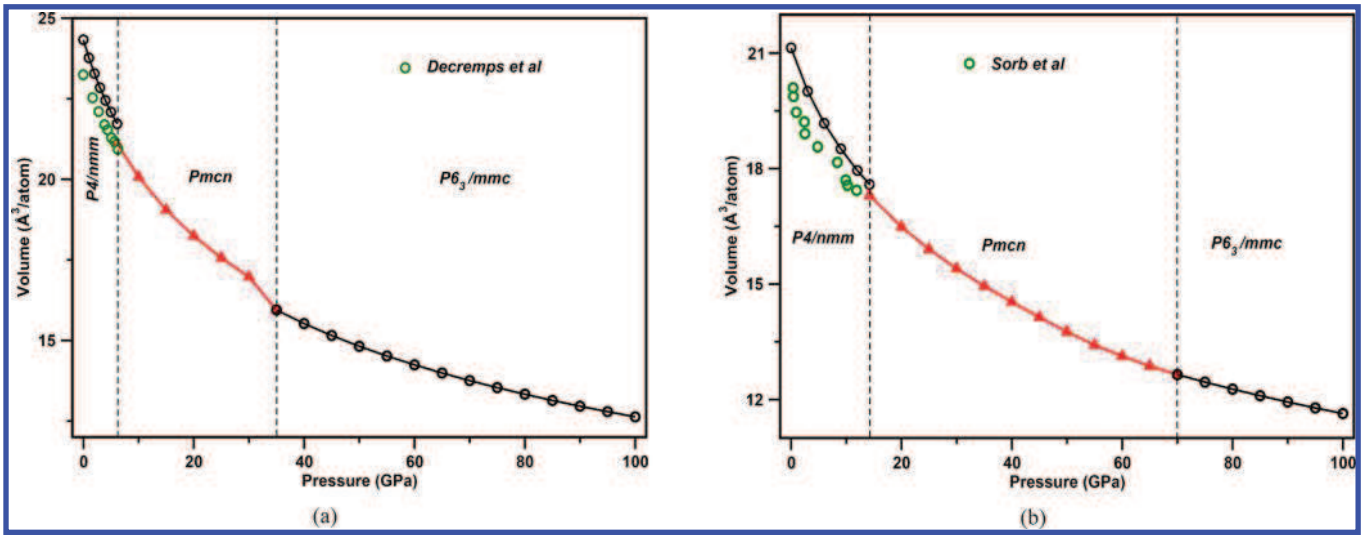

Figure 10. Calculated equilibrium volume as a function of pressure for ambient and high pressure phases of (a) BaClF and (b) PbClF compounds. *P4/nmm* → *Pmcn* transition is first order in nature with volume collapse of 2.8% and 1.6% for BaClF and PbClF, respectively while the *Pmcn* → $P6_3/mmc$ transition is weak first order with displacive nature.

DOI: 10.1021/acs.inorgchem.9b00243
Inorg. Chem. 2019, 58, 5886−5899

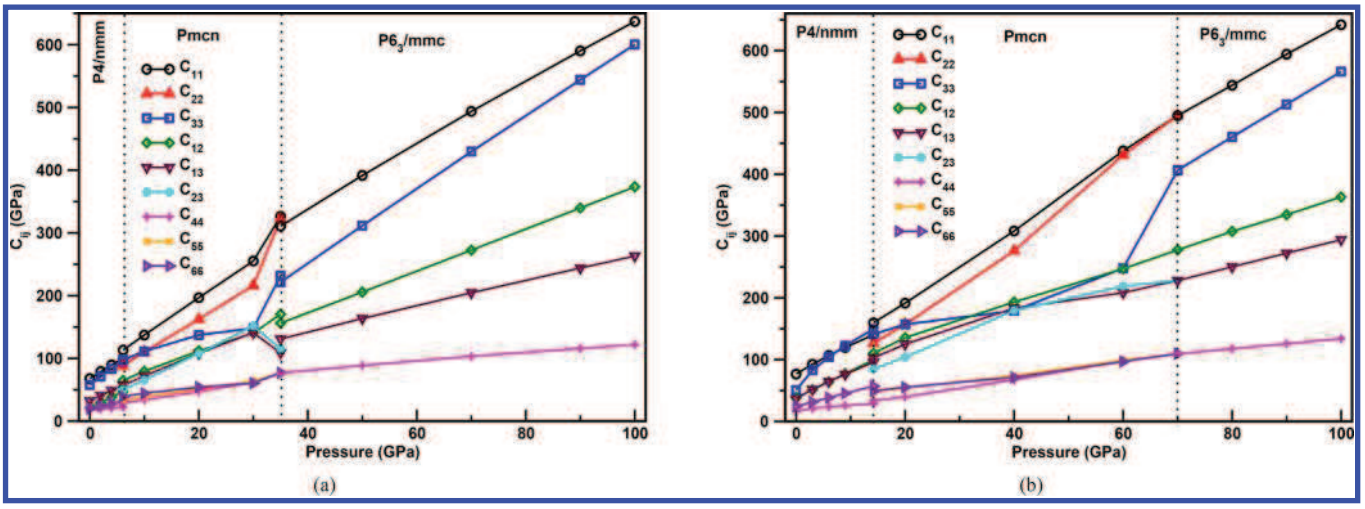

Figure 11. Calculated second order elastic constants (C_{ij}) as a function of pressure for low ($P4/nmm$) and high ($Pmcn$, $P6_3/mmc$) pressure phases of (a) BaClF and (b) PbClF compounds. Merging of nine independent orthorhombic elastic constants with five independent hexagonal elastic constants clearly demonstrates the martensitic nature of $Pmcn \rightarrow P6_3/mmc$ transition under high pressure.

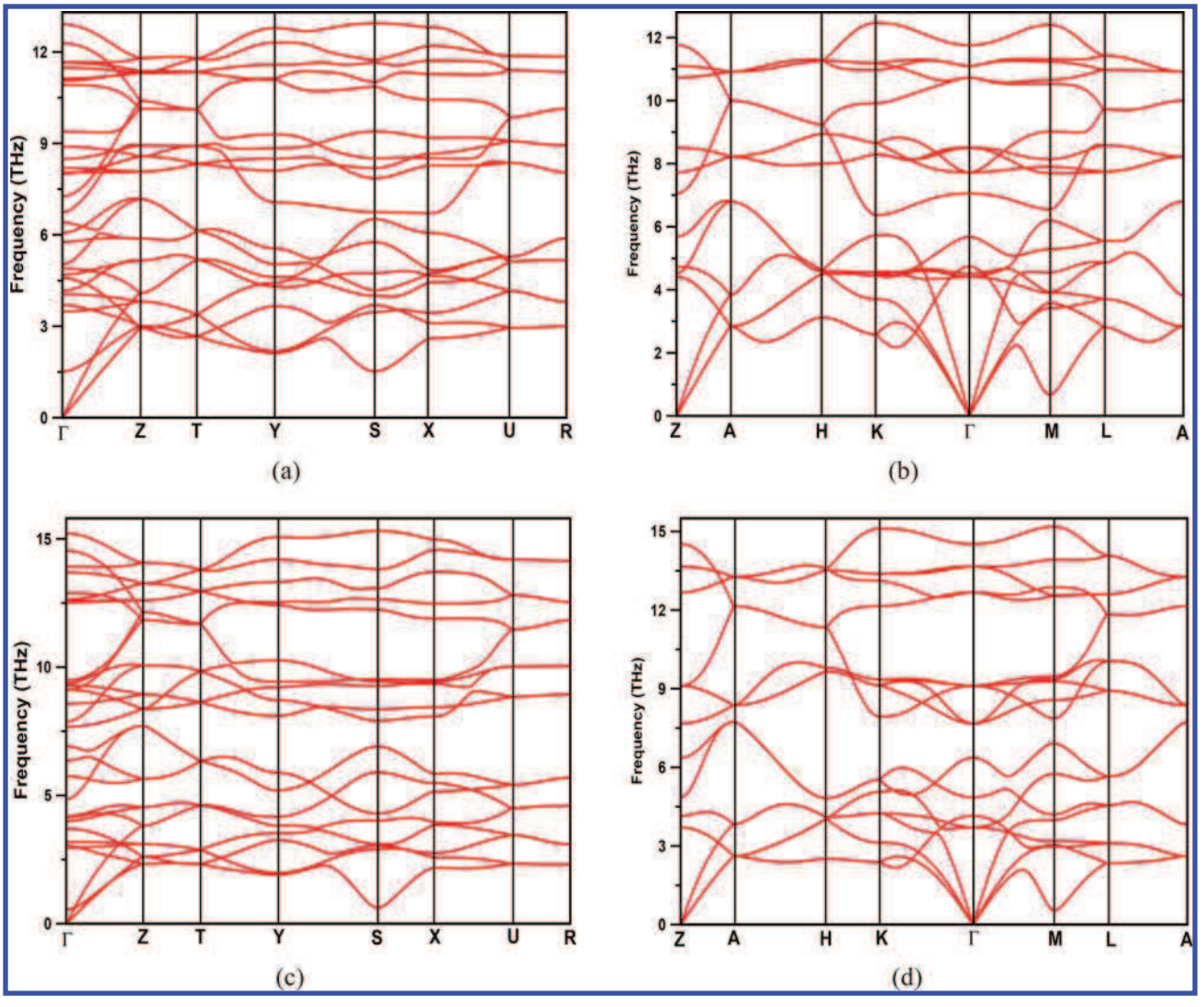

Figure 12. Dynamical stability of the predicted high pressure phases for BaClF and PbClF are explored from the calculated phonon dispersion curves (a) at 40 GPa for $Pmcn$, (b) 35 GPa for $P6_3/mmc$ phases of BaClF, and at 70 GPa for (c) $Pmcn$ and (d) $P6_3/mmc$ phases of PbClF.

Brillouin zone. No imaginary phonon frequencies were found for all the predicted phases at appropriate pressures corresponding to phase transition pressures which clearly demonstrates the dynamical stability of the predicted phases for both of these

DOI: 10.1021/acs.inorgchem.9b00243
Inorg. Chem. 2019, 58, 5886−5899

compounds under investigation (see Figure 12 and Figure S1). The phonon dispersion relations not only provides an information on dynamical stability but also they are essential to understand the nature of structural phase transitions. For instance, the ambient ($P4/nmm$) phase is dynamically stable above the transition pressures (6.1 GPa for BaClF and 14.2 GPa for PbClF), but the intermediate ($Pmcn$) phase is energetically favorable. From the relative enthalpy difference of the predicted phases (see Figure 1), it is very clear that the $P4/nmm \rightarrow Pmcn$ transition is first order in nature, which corroborates with the considerable volume collapse between these two phases during the structural transition. On the other hand, as illustrated in Figure 12a,c, the computed phonon dispersion curves for the $Pmcn$ phase being slightly above the transition pressure clearly shows the softening of acoustic phonon modes across the "S" high symmetry point of the Brillouin zone for the investigated compounds. The observed softening of the acoustic phonon modes above the transition pressure clearly demonstrates that the $Pmcn \rightarrow P6_3/mmc$ transition is first order in nature with very weak volume collapse. The weak first order and displacive nature during the $Pmcn \rightarrow P6_3/mmc$ transition suggests that the pressure induced martensite phase transformation in both of the studied MClF compounds.

Electronic Structure and Optical Properties under High Pressure. TB-mBJ potential and its new parametrization have been used to investigate the electronic structure and optical properties at ambient as well as high pressure. We could predict reasonably improved band gaps for the ambient phases of the studied compounds over PBE-GGA and EV-GGA functionals,[47,48,56] as presented in Table 4. The obtained band gaps 7.12 (4.94), 7.30 (5.05), and 7.73 (5.31) eV using TB-mBJ, TB-mBJ:1, and TB-mBJ:2 potentials for BaClF (PbClF), respectively. The calculated band gap 5.31 eV for PbClF using TB-mBJ:2 potential is in excellent agreement with the meaured band gap 5.2 eV from the reflection spectra.[57] It is well established from the previous[47,48,55] studies that the BaClF and PbClF compounds are direct band gap insulators along Γ- and Z-high symmetry points, respectively, and the present study results are consistent with the previously reported ones (see Figures S2a and S3a). The direct band gap nature is very well reproduced by TB-mBJ:2 potential for BaClF, whereas the top of the valence band is shifted to X high symmetry point (becomes flat along Z-high symmetry point) relative to the PBE-GGA functional for PbClF. In the case of BaF_2,[58] the minimum of the conduction band is shifted from Γ to X high symmetry point using original TB-mBJ potential relative to PBE-GGA functional. However, the predicted band profiles for the ambient phases are consistent with our previous study[55] using original TB-mBJ potential as well as with Hasan et al.[47] and Reshak et al.[48] studies using EV-GGA potentials. The inclusion of spin−orbit coupling (SOC) has a minor effect on the electronic structure of the ambient phase of PbClF, except a small shift in the conduction bands, as illustrated in Figure S2b. Especially, the top valence band in mixed alkaline-earth halofluorides[55,59] are well separated into two distinct manifolds due to the electronegativity difference between the flourine and other halogen (Cl, Br, and I) atoms. This separation increases from Cl → Br → I and Ca → Sr → Ba in MXF (M = Ca, Sr, and Ba and X = Cl, Br, and I) compounds due to increase in atomic number which increase the electronegativity difference between F and other halogens (Cl, Br, and I).[55,59] For instance, the two manifolds are touching each other in BaIBr,[58] while they are well separated in MXF (M = Ca, Sr, Ba, and Pb and X = Cl, Br, and I), except MClF (M = Ca, Sr and Pb) compounds.[59,47] This clearly shows a metal cation also plays an important role in determining the separation between these two manifolds. The close separation of $Cl-p$ and $F-p$ manifolds, similar to that of BaIBr, stopping power due to its high density (7.11 g/cm^3), reasonably good light yield of 2% to that of BGO, and slow and fast decay times are favorable for PbClF to be a good inorganic scintillator.[57] The separation of this manifold in alkaline-earth mixed halofluorides such as MXF (M = Pb, Ca, Sr, and Ba, and X = Cl, Br, and I) shows different responses to the ionizing radiation when compared to highlighted output scintillators such as BaIBr[61,60] and SrI_2,[62] and also, the possible mechanism for this distinct response is discussed in a detailed manner in our previous study.[55]

Table 4. Calculated Electronic Band Gap of Ambient Phase Using Various New Parameterizations of TB-mBJ Potentials and Are Compared with the Available Experimental Data and Other Previous Calculations

work	method	BaClF	PbClF
this work	PBE-GGA	5.42	3.54
	TB-mBJ	7.12	4.94
	TB-mBJ:1	7.30	5.05
	TB-mBJ:2	7.73	5.31
expt			5.2[a]
others	PBE-GGA	5.36,[b] 5.41[c]	3.49,[b] 3.5[a]
	LDA	5.08[b]	3.23[b]
	EV-GGA	6.22[b]	4.28,[b] 4.32[d]
	TB-mBJ	7.10[c]	
	GW		5.0[a]
	TB-LMTO	7.07[e]	

[a]Ref 57. [b]Ref 47. [c]Ref 55. [d]Ref 48. [e]Ref 56.

Moreover, high pressure not only tunes magnitude of band gap but also changes its direct/indirect band gap nature for high pressure phases of BaClF and PbClF. The calculated band gap decreases with pressure for all three predicted phases of these two compounds. BaClF (7.2 eV) and PbClF (5.3 eV) are wide band gap insulators at ambient pressure and reduce their band gaps to ∼3.0−2.5 eV (see Figure 13) for the high pressure $P6_3/mmc$ phase at 100 GPa. This indicates an insulating to semiconducting nature of these materials under high pressure and it may be expected to exhibit metallization upon further compression to ultrahigh pressures. As shown in Figure S3, the predicted high pressure $Pmcn$ and $P6_3/mmc$ phases show the direct band gap nature along Γ−Γ for BaClF, while they are indirect band gap insulators for PbClF along S−T and M−Γ high symmetry points, respectively. As illustrated in Figure S3 and Figure 14, the top of valence $Cl-p$ and $F-p$ band profiles of high pressure phases also merge with pressure in contrast to the ambient phase due to delocalization of electrons, which increases the hybridization between $Cl-p$ and $F-p$ states, and this behavior is much more pronounced in PbClF over BaClF under high pressure.

In order to get insight on the optical isotropic nature of the investigated materials, we have calculated the refractive index of BaClF and PbClF for low and high pressure phases as a function of photon energy, as shown in Figure 15. The calculated static refractive indices at ambient pressure are $n_{xx} = 1.541$, $n_{zz} = 1.535$ and $n_{xx} = 1.832$, $n_{zz} = 1.755$ for BaClF and PbClF, respectively, and the corresponding differences of refractive indices between the a and c crystallographic axes are ∼0.4 and 4.2%. In addition,

DOI: 10.1021/acs.inorgchem.9b00243
Inorg. Chem. 2019, 58, 5886−5899

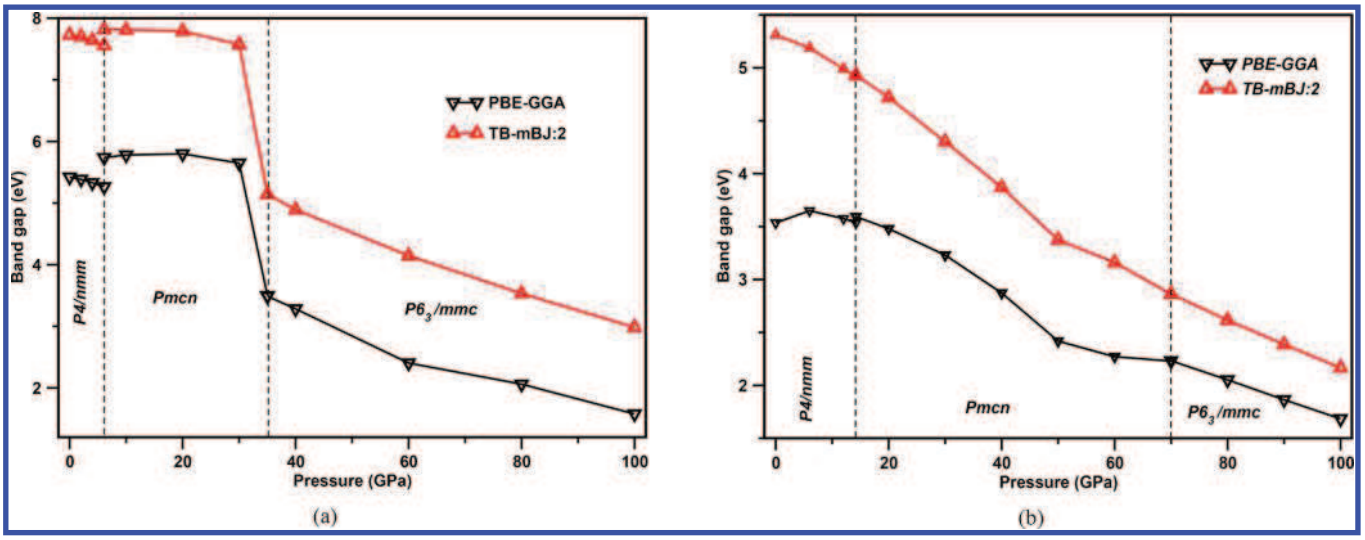

Figure 13. Calculated electronic band gap as a function of pressure for low (*P*4/*nmm*) and high (*Pmcn*, *P*6$_3$/*mmc*) pressure phases of (a) BaClF and (b) PbClF compounds. The band gap decreases with pressure for all three phases in both of the investigated compounds.

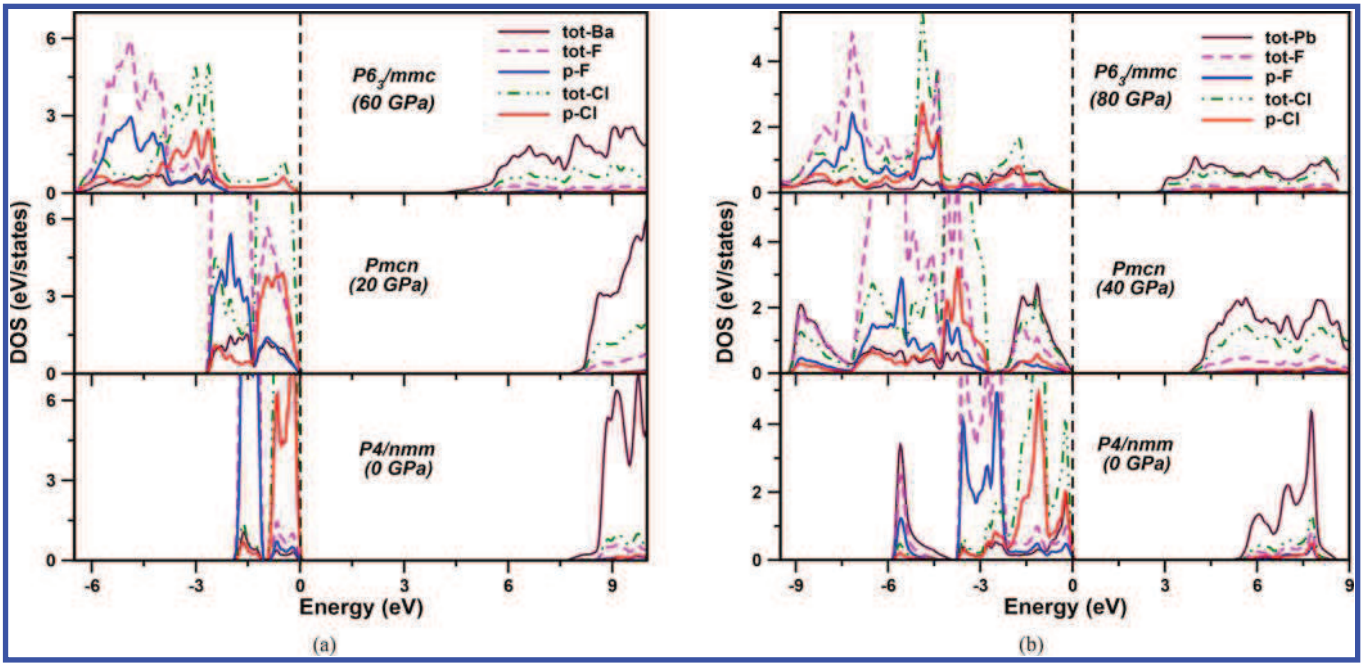

Figure 14. Calculated electronic partial density of states as a function of pressure for low (*P*4/*nmm*) and high (*Pmcn*, *P*6$_3$/*mmc*) pressure phases of (a) BaClF and (b) PbClF compounds. The delocalization of electrons in high pressure phases due to overlap of orbitals under high pressure.

we could clearly observe weak and strong optical anisotropy for BaClF and PbClF compounds for ambient phase even at high pressures (see Figure 15). Also, the ambient phase of PbClF shows strong optical anisotropy when compared to other mixed halofluorides such as MXF (M = Ca, Sr, and Ba and X = Cl, Br, and I).[59] As expected, the refractive index increases as the band gap decreases with pressure for all the phases for both of the studied compounds. As illustrated in Figure 15, optical anisotropy becomes weak from *P*4/*nmm* → *Pmcn* → *P*6$_3$/*mmc* for PbClF; in contrast, optical anisotropy is enhanced from low to high pressure phases of BaClF. Despite the fact that all the predicted phases, including ambient phase, are structurally anisotropic, they exhibit nearly isotropic optical properties, which is a favorable situation for the production of transparent ceramic storage phosphors.

CONCLUSIONS

In summary, we have systematically searched the crystal structures of PbClF-type compounds with 2, 4, and 8 formula units per primitive cell at ambient as well as high pressure using an ab initio evolutionary approach. We predict three stable phases (*P*4/*nmm*, *Pmcn*, and *P*6$_3$/*mmc*) within the studied pressure range. The *P*4/*nmm* → *Pmcn* transition is found to be first order in nature, with an associated volume collapse of ∼2.8% at 6.1 GPa for BaClF and ∼1.6% at 14.2 GPa for PbClF. Interestingly, the *Pmcn* → *P*6$_3$/*mmc* transition is a weak first order and of displacive nature. We propose two mechanisms that mainly drive the martensite (*Pmcn* → *P*6$_3$/*mmc*) phase transformation: (1) tilting and transformation distorted heptahedron to pentahedron environment of Cl^- ions around a metal cation (MCl_6) leads to negative area compressibility and (2) cooperative displacive movement of F^- ions to form a

DOI: 10.1021/acs.inorgchem.9b00243
Inorg. Chem. 2019, 58, 5886−5899

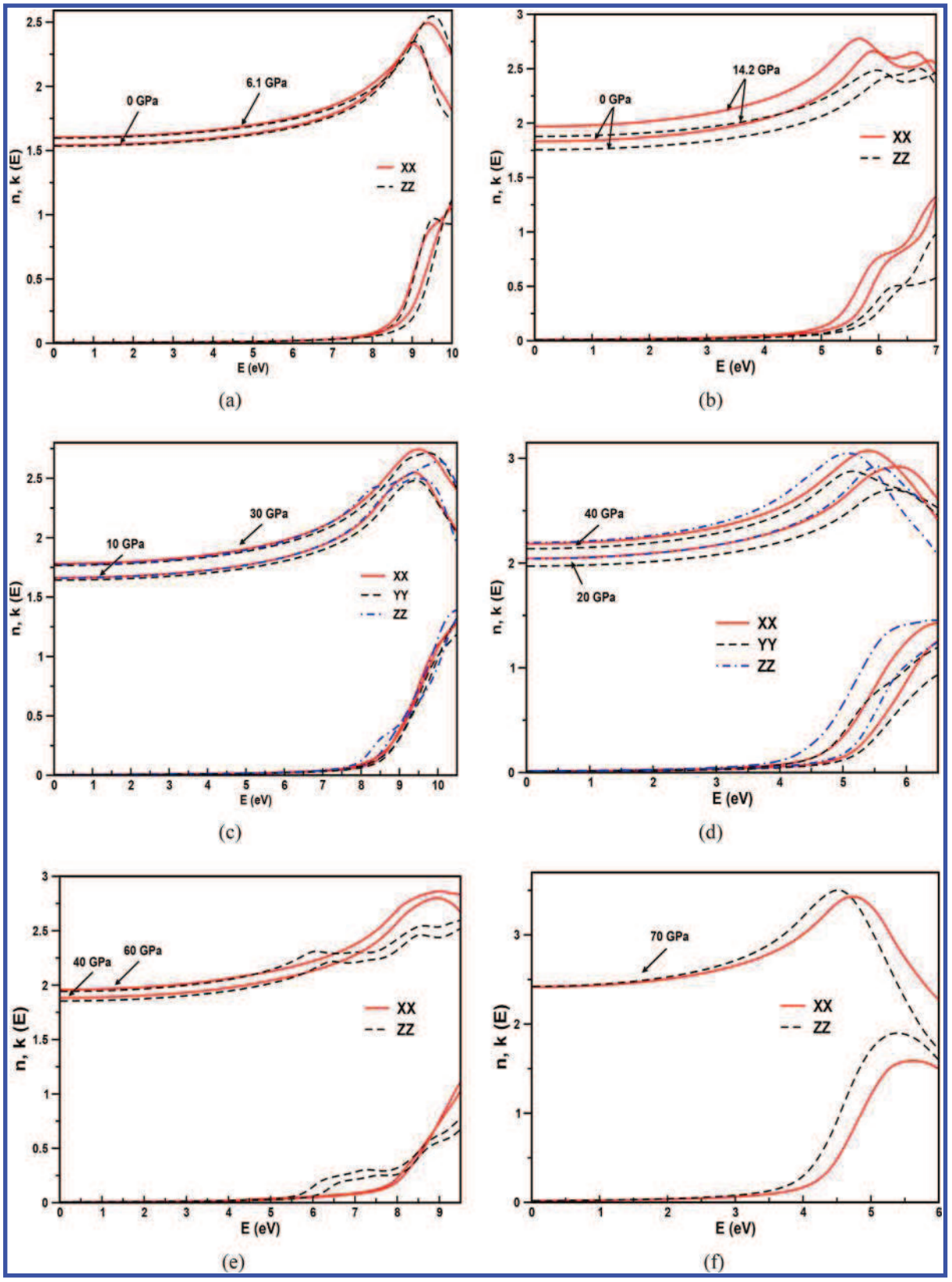

Figure 15. Calculated refractive index of low (a, b) *P*4/*nmm* and high (c, d) *Pmcn*. (e, f) $P6_3/mmc$ pressure phases of BaClF (left) and PbClF (right) compounds as a function of photon energy and pressure. The predicted high pressure (*Pmcn* and $P6_3/mmc$) phases show nearly isotropic optical properties for both of the investigated compounds under high pressure.

trigonal bypyramidal structure (MF_5). Austenite and martensite phases have a common habit (*ab*)-plane, and these two phases are energetically competitive in a wide pressure range, especially for the PbClF compound, which makes it difficult for experimentalist to resolve the high pressure phase. The computed second order elastic constants as a function of

DOI: 10.1021/acs.inorgchem.9b00243
Inorg. Chem. 2019, 58, 5886−5899

pressure show the mechanical stability of all the predicted phases under high pressure. The three predicted phases for BaClF and the ambient phase of PbClF are found to be direct band gap insulators, while the high pressure phases of PbClF are indirect band gap insulators. The top of valence *Cl*−*p* and *F*−*p* manifolds are well separated in the case of BaClF, whereas the two manifolds are close to each other in PbClF, analogous to BaIBr. We could see a strong hybridization between Cl and F derived manifolds in high pressure phases, which is due to delocalization of electrons under high pressure. We predict nearly isotropic optical properties for all the predicted phases (except the ambient phase of PbClF, which shows strong anisotropy relative to the ambient phase of BaClF) with anisotropic crystal structures. Finally, the predicted high pressure phases of (Ba/Pb)ClF compounds provide good insights to determine crystal structures of PbClF- and ZrSiS-type materials.

■ ASSOCIATED CONTENT

Supporting Information

The Supporting Information is available free of charge on the ACS Publications website at DOI: 10.1021/acs.inorgchem.9b00243.

Phonon dispersions of ambient (*P*4/*nmm*) and intermediate (*Pmcn*) phases (Figure S1), electronic band structures (Figure S2 and S3), ground state structural properties in $P2_1/m$ (Table S1) and *Pnma* (Table S2) symmetries, and calculated elastic (Table S4) and polycrystalline (Table S3) properties of MClF compounds (PDF)

■ AUTHOR INFORMATION

Corresponding Author

*E-mail: nykondalu@gmail.com

ORCID

N. Yedukondalu: 0000-0002-7650-7567

Notes

The authors declare no competing financial interest.

■ ACKNOWLEDGMENTS

N.Y.K. would like to thank the Science and Engineering Research Board and Indo-US Scientific Technology Forum for providing financial support through SERB Indo-US postdoctoral fellowship. N.Y.K. would like to express gratitude to postdoc advisor Prof. Artem R. Oganov for his valuable comments and suggestions. M.M.D.E. thanks the National Science Foundation (EAR-1723160) for supporting this work. Computations were mainly performed on the cluster (QSH) in our laboratory at Stony Brook University, NY, U.S.A.

■ REFERENCES

(1) Flahaut, J. Les Structures Type PbFCl (EOI) et Type Anti-Fe_2As (C38) Des Composés Ternaires á Deux Anions MXY. *J. Solid State Chem.* **1974**, *9* (2), 124−131.

(2) Onken, H.; Vierheilig, K.; Hahn, H. About Silicide and Germanide Chalcogenides of Zirconium and Hafnium. *Z. Anorg. Allg. Chem.* **1964**, *333* (4−6), 267−279.

(3) Wang, C.; Hughbanks, T. Main Group Element Size and Substitution Effects on the Structural Dimensionality of Zirconium Tellurides of the ZrSiS Type. *Inorg. Chem.* **1995**, *34* (22), 5524−5529.

(4) Comodi, P.; Zanazzi, P. F. Improved Calibtration Curve for the Sm^{2+}:BaFCl Pressure Sensor. *J. Appl. Crystallogr.* **1993**, *26* (6), 843−845.

(5) Takahashi, K.; Kohda, K.; Miyahara, J.; Kanemitsu, Y.; Amitani, K.; Shionoya, S. Mechanism of Photostimulated Luminescence in BaFX:Eu^{2+} (X = Cl, Br) Phosphors. *J. Lumin.* **1984**, *31*−*32*, 266−268.

(6) Chen, J.; Shen, D.; Ren, G.; Mao, R.; Yin, Z. A High-Density Inorganic Scintillator: Lead Fluoride Chloride. *J. Phys. D: Appl. Phys.* **2004**, *37* (6), 938−941.

(7) Piermarini, G. J.; Block, S.; Barnett, J. D. Hydrostatic Limits in Liquids and Solids to 100 Kbar. *J. Appl. Phys.* **1973**, *44* (12), 5377−5382.

(8) Xu, Q.; Song, Z.; Nie, S.; Weng, H.; Fang, Z.; Dai, X. Two-Dimensional Oxide Topological Insulator with Iron-Pnictide Superconductor LiFeAs Structure. *Phys. Rev. B: Condens. Matter Mater. Phys.* **2015**, *92* (20), 205310.

(9) Beck, H. P.; Limmer, A.; Denner, W.; Schulz, H. IUCr. Influence of High Hydrostatic Pressure on the Crystal Structure of BaFCl in the Pressure Range up to 6.5 GPa. *Acta Crystallogr., Sect. B: Struct. Sci.* **1983**, *39* (4), 401−404.

(10) Subramanian, N.; Chandra Shekar, N. V.; Sahu, P. C.; Yousuf, M.; Govinda Rajan, K. Crystal Structure of the High-Pressure Phase of BaFCl. *Phys. Rev. B: Condens. Matter Mater. Phys.* **1998**, *58* (2), R555−R558.

(11) Shen, Y. R.; Englisch, U.; Chudinovskikh, L.; Porsch, F.; Haberkorn, R.; Beck, H. P.; Holzapfel, W. B. A Structural Study on the PbFCl-Type Compounds MFCl (M = Ba, Sr and Ca) and BaFBr under High Pressure. *J. Phys.: Condens. Matter* **1994**, *6* (17), 3197−3206.

(12) Decremps, F.; Fischer, M.; Polian, A.; Itié, J. P.; Sieskind, M. Ionic Layered PbFCl-Type Compounds under High Pressure. *Phys. Rev. B: Condens. Matter Mater. Phys.* **1999**, *59* (6), 4011−4022.

(13) Decremps, F.; Gauthier, M.; Chervin, J.-C.; Fischer, M.; Polian, A. Unexpected Value of Transition Pressure in the Ionic Layered BaFI Compound Observed by Raman Scattering. *Phys. Rev. B: Condens. Matter Mater. Phys.* **2002**, *66* (2), No. 024115.

(14) Decremps, F.; Fischer, M.; Polian, A.; Itié, J. P.; Sieskind, M. Prediction of Cell Variations with Pressure of Ionic Layered Crystal Application to the Matlockite Family. *Eur. Phys. J. B* **1999**, *9* (1), 49−57.

(15) Decremps, F.; Fischer, M.; Polian, A.; Sieskind, M. Elasticity of BaFCl Single Crystal under Hydrostatic Pressure. *Eur. Phys. J. B* **1998**, *5* (1), 7−13.

(16) Liu, M.; Kurobori, T.; Hirose, Y. Molecular Dynamics Simulations of the High-Pressure Phase Transitions in BaFCl. *Phys. Status Solidi B* **2001**, *225* (2), R20−R21.

(17) Sundarakannan, B.; Ravindran, T.; Kesavamoorthy, R.; Satyanarayana, S. V. High Pressure Raman Spectroscopic Study of BaFCl. *Solid State Commun.* **2002**, *124* (10−11), 385−389.

(18) Subramanian, N.; Chandra Shekar, N.; Sahu, P. C.; Govinda Rajan, K.; Ruoff, A. Evidence of an Intermediate High-Pressure Phase in BaFBr and BaFI. *Phys. B* **2004**, *351* (1−2), 5−10.

(19) Sorb, Y. A.; Subramanian, N.; Ravindran, T. R. High Pressure Raman Spectroscopy of Layered Matlockite, PbFCl. *J. Phys.: Condens. Matter* **2013**, *25* (15), 155401.

(20) Sorb, Y. A.; Sornadurai, D. Structural Phase Transitions of Ionic Layered PbFX (X = Cl or Br) Compounds under High Pressure. *Mater. Res. Bull.* **2015**, *65*, 1−6.

(21) Singha, R.; Samanta, S.; Chatterjee, S.; Pariari, A.; Majumdar, D.; Satpati, B.; Wang, L.; Singha, A.; Mandal, P. Probing Lattice Dynamics and Electron-Phonon Coupling in the Topological Nodal-Line Semimetal ZrSiS. *Phys. Rev. B: Condens. Matter Mater. Phys.* **2018**, *97* (9), 094112.

(22) Zhou, D.; Li, Q.; Ma, Y.; Cui, Q.; Chen, C. Unraveling Convoluted Structural Transitions in SnTe at High Pressure. *J. Phys. Chem. C* **2013**, *117* (10), 5352−5357.

(23) Oganov, A. R.; Glass, C. W. Crystal Structure Prediction Using Ab Initio Evolutionary Techniques: Principles and Applications. *J. Chem. Phys.* **2006**, *124* (24), 244704.

(24) Lyakhov, A. O.; Oganov, A. R.; Stokes, H. T.; Zhu, Q. New Developments in Evolutionary Structure Prediction Algorithm USPEX. *Comput. Phys. Commun.* **2013**, *184* (4), 1172−1182.

DOI: 10.1021/acs.inorgchem.9b00243
Inorg. Chem. 2019, 58, 5886−5899

(25) Oganov, A. R.; Lyakhov, A. O.; Valle, M. How Evolutionary Crystal Structure Prediction Works-and Why. *Acc. Chem. Res.* **2011**, *44* (3), 227−237.
(26) Kresse, G.; Furthmuller, J. Efficient Iterative Schemes for Ab Initio Total-Energy Calculations Using a Plane-Wave Basis Set. *Phys. Rev. B: Condens. Matter Mater. Phys.* **1996**, *54* (16), 11169−11186.
(27) Kresse, G.; Joubert, D. From Ultrasoft Pseudopotentials to the Projector Augmented-Wave Method. *Phys. Rev. B: Condens. Matter Mater. Phys.* **1999**, *59* (3), 1758−1775.
(28) Perdew, J. P.; Burke, K.; Ernzerhof, M. Generalized Gradient Approximation Made Simple. *Phys. Rev. Lett.* **1996**, *77* (18), 3865−3868.
(29) Togo, A.; Oba, F.; Tanaka, I. First-Principles Calculations of the Ferroelastic Transition between Rutile-Type and $CaCl_2$-Type SiO_2 at High Pressures. *Phys. Rev. B: Condens. Matter Mater. Phys.* **2008**, *78* (13), 134106.
(30) Monkhorst, H. J.; Pack, J. D. Special Points for Brillouin-Zone Integrations. *Phys. Rev. B* **1976**, *13* (12), 5188−5192.
(31) https://github.com/MahdiDavari/FPTE.
(32) Tran, F.; Blaha, P. Accurate Band Gaps of Semiconductors and Insulators with a Semilocal Exchange-Correlation Potential. *Phys. Rev. Lett.* **2009**, *102* (22), 226401.
(33) Blaha, P.; Schwarz, K.; Madsen, G. K. H.; Kvasnicka, D.; Luitz, J. *WIEN2K, an Augmented Plane Wave + Local Orbitals Program for Calculating Crystal Properties*, 2nd ed.; Vienna University of Technology: Vienna, 2001.
(34) Koller, D.; Tran, F.; Blaha, P. Improving the Modified Becke-Johnson Exchange Potential. *Phys. Rev. B: Condens. Matter Mater. Phys.* **2012**, *85* (15), 155109.
(35) Olson, G. B.; Olson, G. B.; Owen, W. S. *Martensite*; ASM International, 1992.
(36) Otsuka, K.; Wayman, C. M. *Shape Memory Materials*; Cambridge University Press, 1998.
(37) Bhattacharya, K.; Conti, S.; Zanzotto, G.; Zimmer, J. Crystal Symmetry and the Reversibility of Martensitic Transformations. *Nature* **2004**, *428* (6978), 55−59.
(38) Umemoto, K.; Wentzcovitch, R. M. Potential Ultrahigh Pressure Polymorphs of ABX_3-Type Compounds. *Phys. Rev. B: Condens. Matter Mater. Phys.* **2006**, *74* (22), 224105.
(39) Umemoto, K.; Wentzcovitch, R. M.; Weidner, D. J.; Parise, J. B. $NaMgF_3$: A Low-Pressure Analog of $MgSiO_3$. *Geophys. Res. Lett.* **2006**, *33* (15), L15304.
(40) Jakymiw, C.; Vocadlo, L.; Dobson, D. P.; Bailey, E.; Thomson, A. R.; Brodholt, J. P.; Wood, I. G.; Lindsay-Scott, A. The Phase Diagrams of $KCaF_3$ and $NaMgF_3$ by Ab Initio Simulations. *Phys. Chem. Miner.* **2018**, *45* (4), 311−322.
(41) D'Anna, V.; Daku, L. M. L.; Hagemann, H.; Kubel, F. Ionic Layered BaFCl and $Ba_{1-x}Sr_xFCl$ Compounds: Physical- and Chemical-Pressure Effects. *Phys. Rev. B: Condens. Matter Mater. Phys.* **2010**, *82* (2), 024108.
(42) Beck, H. P. A Study on Mixed Halide Compounds MFX (M = Ca, Sr, Eu, Ba; X = Cl, Br, I). *J. Solid State Chem.* **1976**, *17* (3), 275−282.
(43) Rajan, K. G.; Lenus, A. J. X-Ray Excited Optical Luminescence Studies on the System BaXY (X,Y = F, Cl, Br, I). *Pramana* **2005**, *65* (2), 323−338.
(44) Sauvage, M. IUCr. Refinement of the Structures of SrFCl and BaFCl. *Acta Crystallogr., Sect. B: Struct. Crystallogr. Cryst. Chem.* **1974**, *30* (11), 2786−2787.
(45) Kesavamoorthy, R.; Rao, G. V. N.; Sundarakkannan, B.; Ghosh, G.; Sastry, V. S. Powder Diffraction Data of BaFCl. *Powder Diffr.* **1997**, *12* (04), 255−258.
(46) Pasero, M.; Perchiazzi, N. Crystal Structure Refinement of Matlockite. *Mineral. Mag.* **1996**, *60* (402), 833−836.
(47) haj Hassan, F. El; Akbarzadeh, H.; Hashemifar, S. J.; Mokhtari, A. Structural and Electronic Properties of Matlockite MFX (M = Sr, Ba, Pb; X = Cl, Br, I) Compounds. *J. Phys. Chem. Solids* **2004**, *65* (11), 1871−1878.
(48) Reshak, A. H.; Charifi, Z.; Baaziz, H. First-Principles Study of the Optical Properties of PbFX (X = Cl, Br, I) Compounds in Its Matlockite-Type Structure. *Eur. Phys. J. B* **2007**, *60* (4), 463−468.
(49) de la Flor, G.; Orobengoa, D.; Tasci, E.; Perez-Mato, J. M.; Aroyo, M. I. Comparison of structures applying the tools available at the Bilbao Crystallographic Server. *J. Appl. Crystallogr.* **2016**, *49*, 653−664.
(50) Capillas, C.; Perez-Mato, J. M.; Aroyo, M. I. Maximal symmetry transition paths for reconstructive phase transitions. *J. Phys.: Condens. Matter* **2007**, *19*, 275203.
(51) Orobengoa, D.; Capillas, C.; Aroyo, M. I.; Perez-Mato, J. M. AMPLIMODES: symmetry-mode analysis on the Bilbao Crystallographic Server. *J. Appl. Crystallogr.* **2009**, *42*, 820−833.
(52) Bergerhoff, G.; Berndt, M.; Brandenburg, K.; Degen, T. Concerning inorganic crystal structure types. *Acta Crystallogr., Sect. B: Struct. Sci.* **1999**, *B55*, 147−156.
(53) Decremps, F.; Fischer, M.; Polian, A.; Sieskind, M. Sound velocity measurement by ultrasonic and Brillouin scattering techniques in compounds with matlockite structure. *High Temp. - High Pressures* **1998**, *30*, 235−240.
(54) Sieskind, M.; Polian, A.; Fischer, M.; Decremps, F. Some Scaling Factors of Physical Properties Dependent on Phonons in the Case of the Families of the Fluorite and of the Matlockite. *J. Phys. Chem. Solids* **1998**, *59* (1), 75−82.
(55) Yedukondalu, N.; Babu, K. R.; Bheemalingam, C.; Singh, D. J.; Vaitheeswaran, G.; Kanchana, V. Electronic Structure, Optical Properties, and Bonding in Alkaline-Earth Halofluoride Scintillators: BaClF, BaBrF and BaIF. *Phys. Rev. B: Condens. Matter Mater. Phys.* **2011**, *83* (16), 165117.
(56) Kalpana, G.; Palanivel, B.; Shameem Banu, I. B.; Rajagopalan, M. Structural and Electronic Properties of Alkaline-Earth Fluorohalides under Pressure. *Phys. Rev. B: Condens. Matter Mater. Phys.* **1997**, *56* (7), 3532−3535.
(57) Liu, B.; Shi, C.; Yin, M.; Fu, Y.; Shen, D. Electronic, Optical and Luminescent Properties of PbFCl Single Crystal. *J. Phys.: Condens. Matter* **2005**, *17* (33), 5087−5094.
(58) Singh, D. J. Structure and Optical Properties of High Light Output Halide Scintillators. *Phys. Rev. B: Condens. Matter Mater. Phys.* **2010**, *82* (15), 155145.
(59) Kanchana, V.; Yedukondalu, N.; Vaitheeswaran, G. Structural, Elastic, Electronic and Optical Properties of Layered Alkaline-Earth Halofluoride Scintillators. *Philos. Mag.* **2013**, *93* (26), 3563−3575.
(60) Shalaev, A. A.; Shendrik, R.; Myasnikova, A. S.; Bogdanov, A.; Rusakov, A.; Vasilkovskyi, A. Luminescence of BaBrI and SrBrI Single Crystals Doped with Eu^{2+}. *Opt. Mater. (Amsterdam, Neth.)* **2018**, *79*, 84−89.
(61) Bourret-Courchesne, E. D.; Bizarri, G. A.; Borade, R.; Gundiah, G.; Samulon, E. C.; Yan, Z.; Derenzo, S. E. Crystal Growth and Characterization of Alkali-Earth Halide Scintillators. *J. Cryst. Growth* **2012**, *352* (1), 78−83.
(62) van Loef, E. V.; Wilson, C. M.; Cherepy, N. J.; Hull, G.; Payne, S. A.; Choong, W.-S.; Moses, W. W.; Shah, K. S. Crystal Growth and Scintillation Properties of Strontium Iodide Scintillators. *IEEE Trans. Nucl. Sci.* **2009**, *56* (3), 869−872.

DOI: 10.1021/acs.inorgchem.9b00243
Inorg. Chem. 2019, 58, 5886−5899